

The flow of Energy through the Earth's Climate System: Land and Ocean Exchanges

Kevin E Trenberth and John T. Fasullo

NCAR, Boulder, CO, USA

Correspondence: Contact trenbert@ucar.edu

INTRODUCTION

Weather and climate on Earth is determined by the amount and distribution of incoming radiation from the sun. For an equilibrium climate, outgoing longwave radiation (OLR) necessarily balances the incoming absorbed solar radiation (ASR), although there is a great deal of fascinating atmosphere, ocean and land phenomena that couple the two. Incoming radiant energy may be scattered and reflected by clouds and aerosols or absorbed in the atmosphere. The transmitted radiation is then either absorbed or reflected at the Earth's surface. Radiant solar or shortwave energy is transformed into sensible heat, latent energy (involving different water states), potential energy and kinetic energy before being emitted as longwave radiant energy. Energy may be stored for some time, transported in various forms, and converted among the different types, giving rise to a rich variety of weather or turbulent phenomena in the atmosphere and ocean. Moreover, the energy balance can be upset in various ways, changing the climate and associated weather.

In this paper, the mean and annual cycle of energy flowing into the climate system and its storage, release, and transport in the atmosphere, ocean, and land surface are estimated with recent observations. The variability is also considered. An emphasis is placed on establishing internally consistent quantitative estimates with discussion and assessment of uncertainty. At the top-of-atmosphere (TOA), adjusted radiances from Earth Radiation Budget Experiment (ERBE) and Clouds and the Earth's Radiant Energy System (CERES) are used. In the atmosphere, reanalyses from the National Centers for Environmental Prediction/NCAR reanalysis (NRA) (Kalnay et al. 1996) and the second generation European Centre for Medium Range Weather Forecasts (ECMWF) Reanalysis (ERA-40) (Uppala et al. 2005) and recent Japanese Reanalysis (JRA) (Onogi et al. 2007) are used as they contain the most comprehensive estimates of global atmospheric temperature and moisture fields. Vertically-integrated quantities for energy components, the transports, and divergences have been computed and archived.

The net upward surface flux (F_S) over ocean is derived as the residual of TOA and atmospheric energy budgets, and is compared with direct calculations of ocean heat content (O_E) and its tendency ($\delta O_E/\delta t$) from several ocean temperature datasets. The ocean datasets used to diagnose T include the World Ocean Atlas 2005 (WOA, Locarini et al. 2006), the ocean analysis of the Japanese Meteorological Agency Version 6.2 (JMA, Ishii et al. 2006), and the recently corrected Global Ocean Data Assimilation System (GODAS, Behringer 2006), along with some consideration of the ECCO (Estimating the Circulation and Climate of the Ocean) analyses (Stammer et al. 2004).

Over land F_S from a stand-alone simulation of the Community Land Model forced by observed fields is used. Comprehensive depiction of the energy budget during the ERBE (February 1985 to April 1989) and CERES (Mar. 2000 to May 2004) periods are constructed that match estimates of the global, global-ocean, and global-land imbalances. In addition, the annual cycle of the energy budget during both periods is examined and compared with $\delta O_E/\delta t$.

The near balance between net TOA radiation (R_T) and F_S over ocean and thus with O_E , and between R_T and atmospheric total energy divergence over land, are documented both in the mean and for the annual cycle. However, there is an annual mean transport of energy by the atmosphere from ocean to land regions of 2.2 ± 0.1 PW (10^{15} watts) primarily in the northern winter when the transport exceeds 5 PW. The global albedo is dominated by a semiannual

cycle over the oceans, but combines with the large annual cycle in solar insolation to produce a peak in absorbed solar and net radiation in February, somewhat after the perihelion, and with the net radiation 4.3 PW higher than the annual mean, as it is enhanced by the annual cycle of outgoing long-wave radiation that is dominated by land regions. *In situ* estimates of the annual variation of O_E are found to be unrealistically large. Challenges in diagnosing interannual variability in the energy budget and its relationship to climate change are identified in the context of the episodic and inconsistent nature of observations.

RESULTS

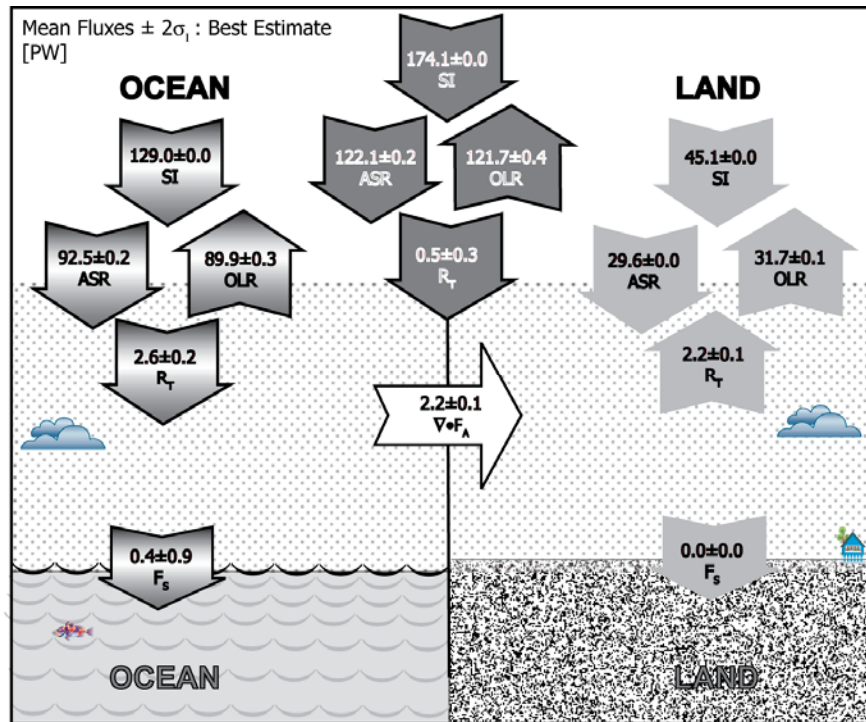


Figure 1: CERES-period March 2000 to May 2004 mean best-estimate TOA fluxes [PW] globally (center grey) and for global-land (right, light grey) and global-ocean (left) regions. SI is the solar irradiance and the net downward radiation $R_T = ASR - OLR$.

In the figure, the arrows show the direction of the flow. The net surface flux is also given along with the energy flow from ocean to land.

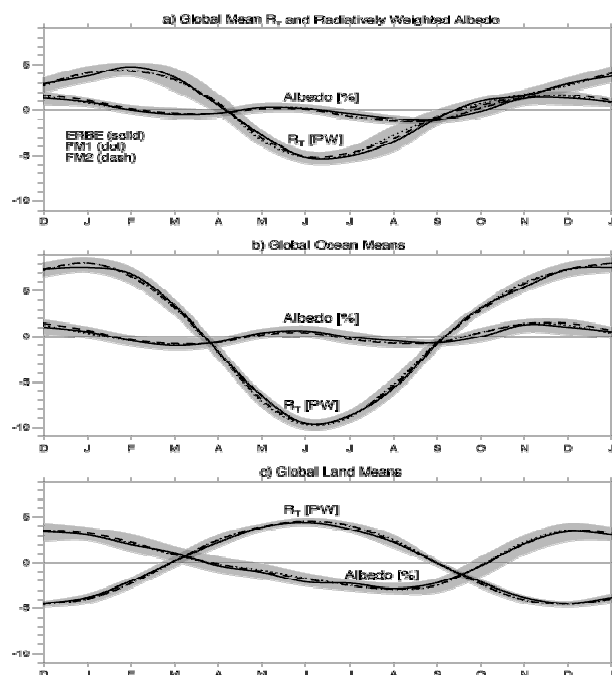


Figure 2: a) Global, b) global-ocean, and c) global-land mean annual cycles of albedo (%) and R_T (PW) where shading represents $\pm 2\sigma_1$ of monthly means and the annual mean has been removed. σ_1 is the standard error from interannual sampling. Values plotted are from ERBE and the two CERES instruments on board Terra (FM1 and FM2). The global albedo drops from January, which is when perihelion occurs, to February, so that peak ASR and net radiation occurs in February. The ocean values tend to follow those in the southern hemisphere which has more ocean, while the land values follow the northern hemisphere. Over ocean, the albedo undergoes a semiannual cycle associated with monsoons and cloud changes. Over land, albedo is highest in winter in association with snow cover variations and the changing irradiance over Antarctica.

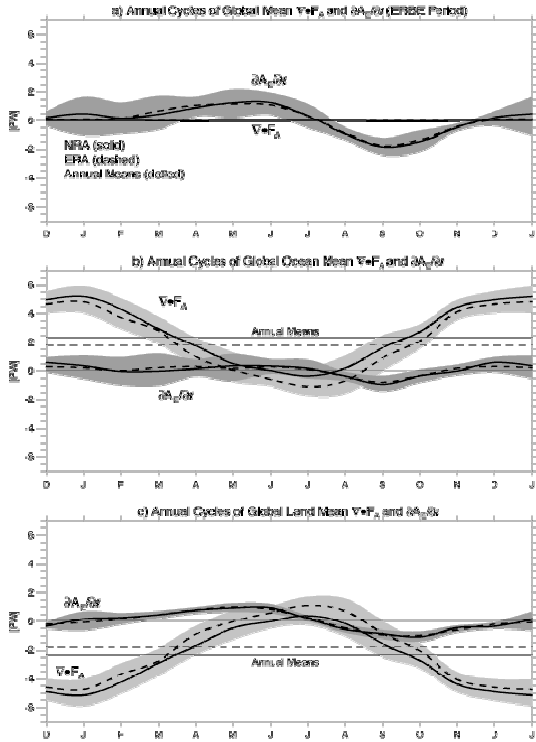


Figure 3: a) Global, b) global-ocean, and c) global-land estimates of atmospheric total energy divergence ($\nabla \cdot F_A$) and tendency ($\partial A_E / \partial t$) are shown in PW where shading represents $\pm 2\sigma_1$ of monthly means and the annual mean is shown (dotted). Globally the atmospheric divergence is identically zero and the ocean and land values are equal but opposite, with maximum transport in northern winter from ocean to land. Atmospheric storage variations are small but not negligible.

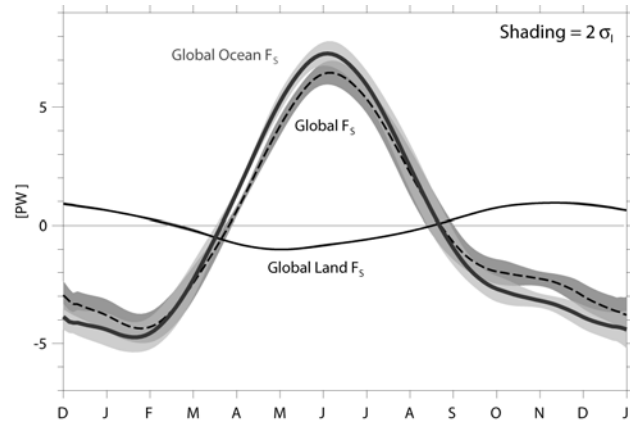


Figure 4 (right): Global, global-ocean, and global-land estimates of net upwards surface flux (F_S) are shown in PW where shading represents $\pm 2\sigma_1$ of monthly means.

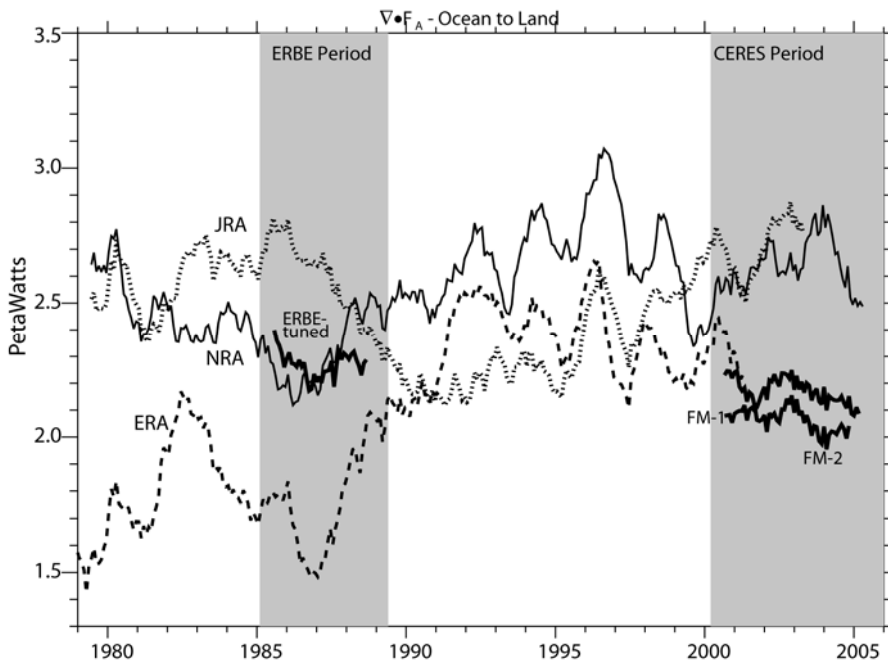


Figure 5: Ocean to land energy transport in PW as 12-month running means inferred from ERBE and CERES R_T over land and NRA $\partial A_E / \partial t$ fields (see text, dark black). Transports from NRA (thin solid), ERA-40 (dashed) and JRA (dotted) fields are also shown. Both ERA-40 and JRA experience major drifts with introduction of SSM/I observations in July 1987 and transitions of NOAA-9 to NOAA 11 in 1988. ERA-40 values jump when Pinatubo erupted in 1991. All values are influenced by the TOVS to ATOVS transition in 1998 (in JRA) to 2001. As is

evident here, agreement is poor among the reanalyses both in absolute terms and for the low frequency variability. The estimates from the satellite products are more realistic but highlight the errors in the changes from the ERBE to CERES periods in the reanalyses.

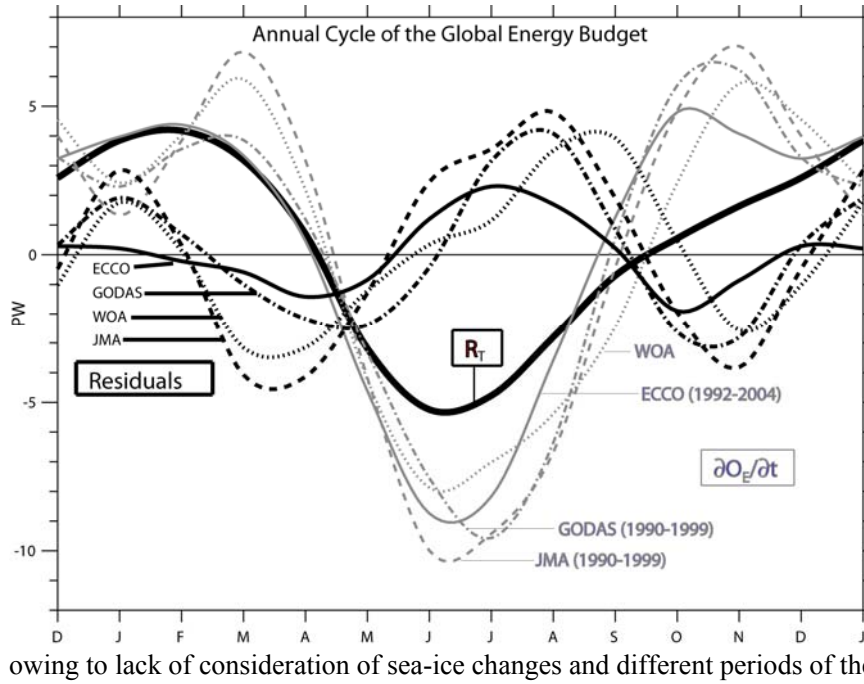


Figure 6. The annual cycle of TOA radiation (heavy black) can be compared with the rates of change in ocean heat content storage (grey curves) from 4 different products. When combined with the radiation and change in land and atmospheric storage, the residual should be zero (black curves). The residuals have a prominent semiannual cycle and are largest for the WOA and JMS products, somewhat improved for GODAS and best for ECCO. Residuals of order 1 PW are not unexpected

owing to lack of consideration of sea-ice changes and different periods of the data.

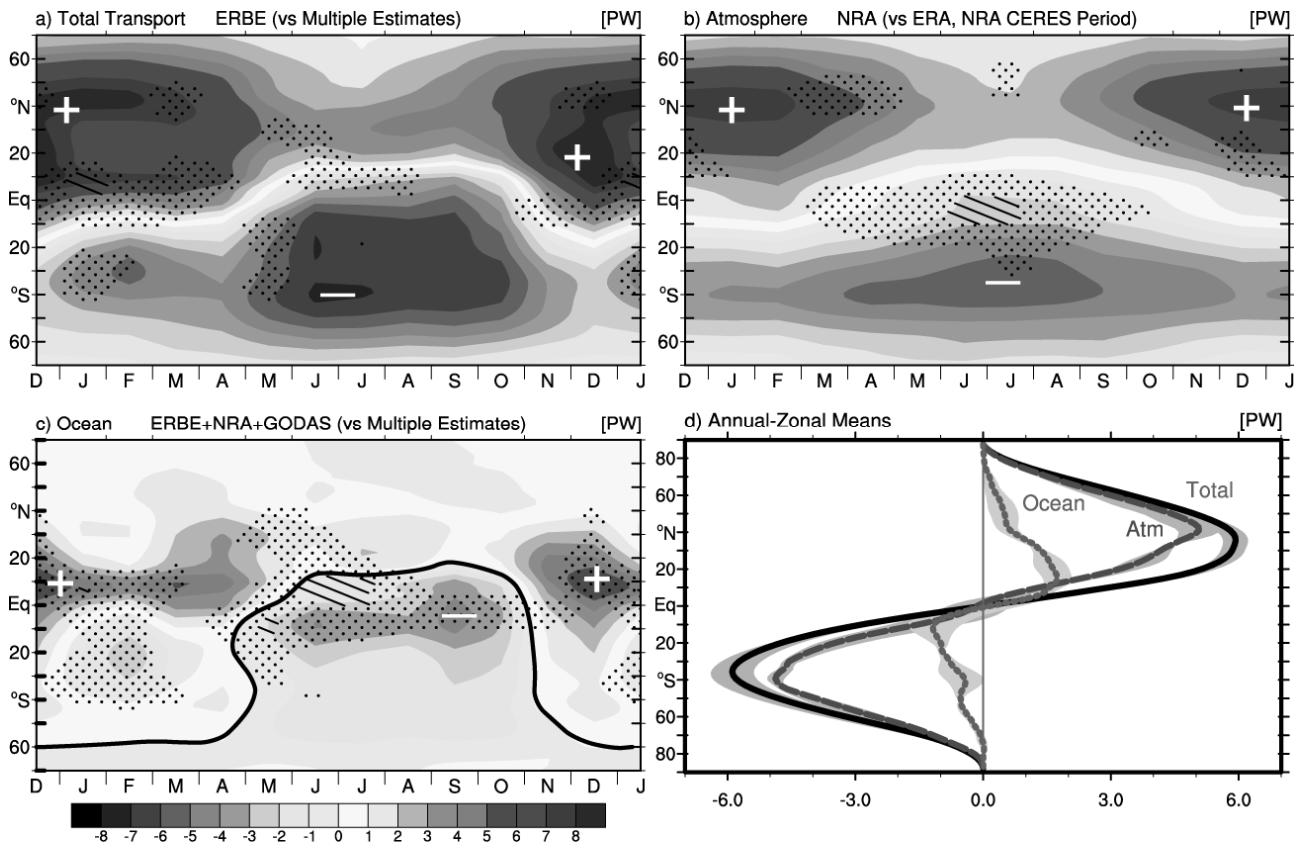


Figure 7: ERBE-period zonal mean annual cycle of meridional energy transport by a) the atmosphere and ocean as inferred from ERBE R_T , NRA $\delta A_E/\delta t$, and GODAS $\delta O_E/\delta t$, b) the atmosphere based on NRA, and c) by the ocean as implied ERBE+NRA F_s and GODAS $\delta O_E/\delta t$. Stippling and hatching in a) through c) represent regions and times of year in which the standard deviation of monthly mean values among estimates, some of which include the CERES period exceeds 0.5 and 1.0 PW, respectively. Also shown (d) is the median annual mean transport by latitude for the total (solid), atmosphere (dashed) and ocean (dotted) accompanied with the associated $\pm 2\sigma$ range (shaded).

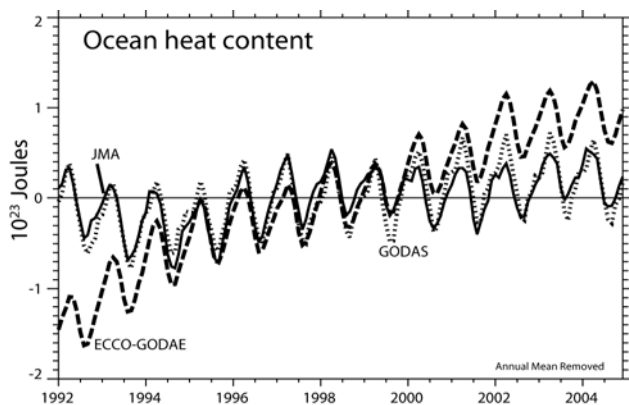


Figure 8. Comparison of the ocean heat content analyses from JMA (solid), GODAS (dotted) and ECCO (dashed) from 1992 to 2006 when altimetry estimates were available of sea level. The long-term mean is removed. An estimated imbalance at TOA of 0.4 PW which goes into the ocean, implies a change of 1.26×10^{23} J/decade, similar to the ECCO changes after 1998. As shown here, the decadal variability is poorly replicated.

This paper is a summary of work mainly documented in three articles. Fasullo and Trenberth (2008a) provide an assessment of the global energy budgets at TOA and the surface, for the global atmosphere, and ocean and land domains based on a synthesis of satellite retrievals, reanalysis fields, a land surface simulation, and ocean temperature estimates. The TOA budget is constrained to match estimates of the global imbalance during recent periods of satellite coverage associated with changes in atmospheric composition and climate. There is an annual mean transport of energy by the atmosphere from ocean to land regions of 2.2 ± 0.1 PW primarily in the northern winter when the transport exceeds 5 PW. Fasullo and Trenberth (2008b) go on to evaluate the meridional structure and transports of energy in the atmosphere, ocean and land for the mean and annual cycle zonal averages over the ocean, land and global domains. Trenberth and Fasullo (2008) delve into the ocean heat budget in considerable detail and provide a comprehensive assessment of uncertainty. As shown here, decadal and longer term variability in both atmosphere and ocean for the energy quantities is poorly replicated and mostly demonstrably wrong. This highlights the challenges for future reanalyses to improve the way the changing observing system affects the results.

REFERENCES

- Behringer, D.W., 2006: The Global Ocean Data Assimilation System (GODAS) at NCEP, Proc. NOAA 31st Ann. Climate Diagnostics Prediction Wkshp, Boulder, CO, October 23-27, 2006.
- Fasullo, J. T., and K. E. Trenberth, 2008a: The annual cycle of the energy budget: Global mean and land-ocean exchanges, *J. Clim.*, in press.
- Fasullo, J. T., and K. E. Trenberth, 2008b: The annual cycle of the energy budget: Meridional Structures, *J. Clim.*, in press.
- Ishii, M., M. Kimoto, K. Sakamoto, and S.I. Iwasaki, 2006: Steric sea level changes estimated from historical ocean subsurface temperature and salinity analyses. *J. Oceanogr.*, **62**, 155-170.
- Kalnay E., and Coauthors, 1996: The NCEP/NCAR 40-year reanalysis project. *Bull. Amer. Meteor. Soc.*, **77**, 437-471.
- Locarnini, R. A., A. V. Mishonov, J. I. Antonov, T. P. Boyer, and H.E. Garcia, 2006. *World Ocean Atlas 2005, Vol. 1: Temperature*. S. Levitus, Ed. NOAA Atlas NESDIS 61, U.S. Gov. Printing Office, Washington, D.C. 182 pp.
- Onogi, K., J. Tsutsui, H. Koide, M. Sakamoto, S. Kobayashi, H. Hatsushika, T. Matsumoto, N. Yamazaki, H. Kamahori, K. Takahashi, S. Kadokura, K. Wada, K. Kato, R. Oyama, T. Ose, N. Mannoji and R. Taira 2007: The JRA-25 Reanalysis. *J. Meteor. Soc. Japan*, **85**, 369-432.
- Stammer D., K. Ueyoshi, A. Köhl, W. G. Large, S. A. Josey, C. Wunsch 2004: Estimating air-sea fluxes of heat, freshwater, and momentum through global ocean data assimilation, *J. Geophys. Res.*, **109**, C05023, doi:10.1029/2003JC002082.
- Trenberth, K. E., and J. Fasullo, 2008: An observational estimate of ocean energy divergence. *J. Phys. Oceanogr.*, in press.
- Uppala, S. M., and coauthors. 2005: The ERA-40 reanalysis. *Quart. J. Roy. Meteor. Soc.*, **131**, 2961-3012.